 doi:10.20944/preprints202112.0058.v1

Type of the Paper (Article)

Electrochemical and Mechanistic Study of Structure–Activity Relationship of α-, β-, γ-, and δ-Tocopherol on Superoxide Elimination in *N*,*N*-Dimethylformamide through Proton-Coupled Electron Transfer

Tatsushi Nakayama [1,*], Ryo Honda [2], Kazuo Kuwata [2], Shigeyuki Usui [1], Bunji Uno [3]

[1] Gifu Pharmaceutical University; Daigaku-nishi, Gifu 501-1196, Japan
[2] United Graduate School of Drug Discovery and Medical Information Sciences, Gifu University; 1-1 Yanagido, Gifu 501-1193, Japan
[3] Faculty of Pharmacy, Gifu University of Medical Science, 4-3-3 Nijigaoka, Kani, Gifu 509–0923, Japan
* Correspondence: tnakayama@gifu-pu.ac.jp; Tel.: +8158-230-8100

Abstract: Elimination of superoxide radical anion ($O_2^{\bullet-}$) by tocopherols (TOH) and related compounds was investigated on the basis of cyclic voltammetry and *in situ* electrolytic electron spin resonance spectrum in *N*,*N*-dimethylformamide (DMF) with the aid of density functional theory (DFT) calculations. Quasi-reversible $O_2/O_2^{\bullet-}$ redox was modified by the presence of TOH, suggesting that the electrogenerated $O_2^{\bullet-}$ was eliminated by α-, β-, γ-TOH through proton-coupled electron transfer (PCET), but not by δ-TOH. The structure–activity correlation of α-, β-, γ-, and δ-TOH characterized by the methyl group on the 6-chromanol ring was experimentally confirmed, where the methyl group promotes the PCET mechanism. Furthermore, comparative analyses using some related compounds suggested that *para*-oxygen-atom in the 6-chromanol ring is required for a successful electron transfer (ET) to $O_2^{\bullet-}$ through the PCET. The electrochemical and DFT results in dehydrated DMF suggested that the PCET mechanism involves preceding proton transfer (PT) forming hydroperoxyl radical followed by a PCET (intermolecular ET–PT). The $O_2^{\bullet-}$ elimination by TOH proceeds efficiently along the PCET mechanism involving one ET and two PTs.

Keywords: proton-coupled electron transfer; superoxide radical anion; antioxidants; cyclic voltammetry; electron spin resonance spectrum; tocopherol

1. Introduction

(2*R*)-2,5,7,8-tetramethyl-2-[(4*R*,8*R*)-4,8,12-trimethyltridecyl]-3,4-dihydro-2H-1-benzopyran-6-ol (α-tocopherol, α-TOH) is one of the most important natural antioxidants within the vitamin E family of compounds. Its characteristic structure is based on 6-chromanol ring with an extended alkyl (phytyl) chain in the 2-position, a fully methylated aromatic ring, and a mono-phenolic group in the 6-position [1–4]. Four structurally related compounds (α-, β-, γ-, and δ-TOH) with saturated phytyl chains are designated as TOH, while tocotrienols are differentiated by the presence of double bonds in the 3', 7', and 11' positions of the alkyl side chain. Currently, the antioxidant property of vitamin E is considered as due to electron donation, which directly eliminates any reactive oxygen species (ROS). Moreover, the increasing number of methyl group on the 6-chromanol ring correlates with the promotion of the antioxidant activities, indicating that α-TOH has the highest value in a di(phenyl)-(2,4,6-trinitrophenyl)iminoazanium radical scavenging assessment [5]. Thus, the redox behavior of vitamin E has been extensively investigated to elucidate the ROS elimination mechanism and any related biochemical reactions [3,6–8].

Preprints (www.preprints.org) | NOT PEER-REVIEWED | Posted: 3 December 2021 doi:10.20944/preprints202112.0058.v1

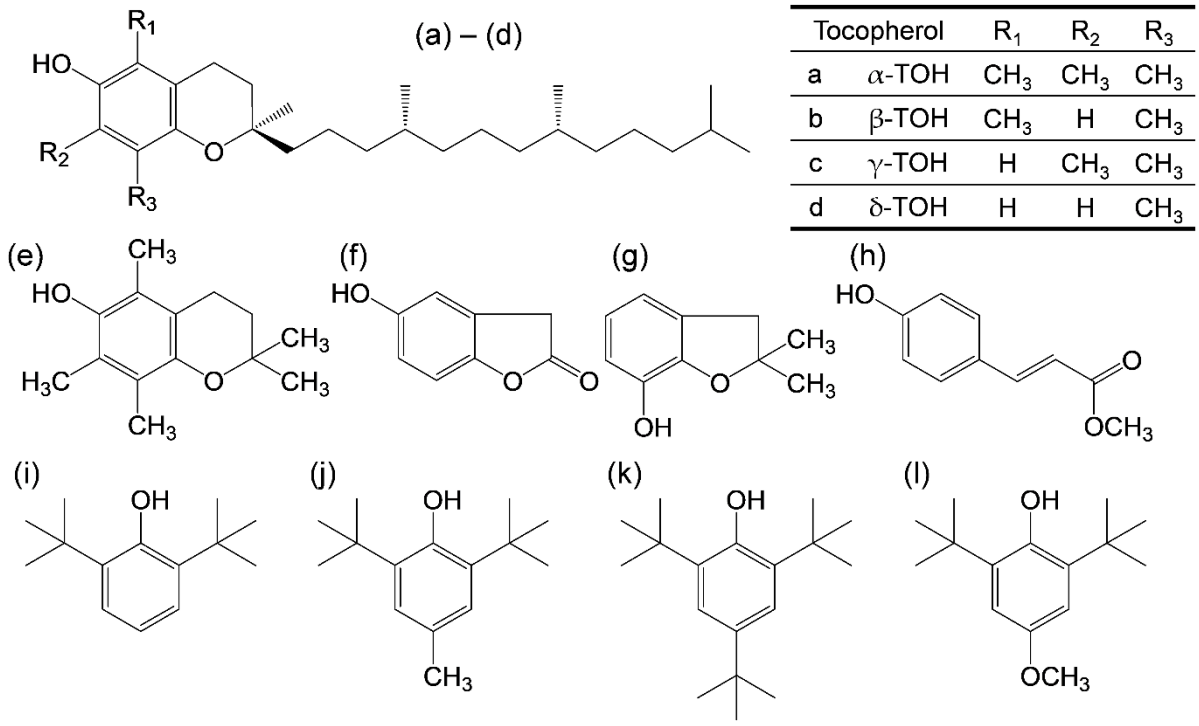

Tocopherol		R_1	R_2	R_3
a	α-TOH	CH_3	CH_3	CH_3
b	β-TOH	CH_3	H	CH_3
c	γ-TOH	H	CH_3	CH_3
d	δ-TOH	H	H	CH_3

Figure 1. Structures of TOH and the related compounds considered in this study. (a)–(d) α-, β-, γ-, and δ-TOH, (e) 2,2,5,7,8-pentamethyl-6-chromanol, (f) homogentisic acid γ-lactone, (g) 2,3-dihydro-2,2-dimethyl-7-hydroxybenzofuran, (h) trans-*para*-coumaric acid, (i) 2,6-di-tert-butyl-phenol (2,6-DTBP), (j) 2,6-di-tert-butyl-4-methylphenol (2,6-DTBM), (k) 2,4,6-tri-tert-butyl-phenol (TTBP), and (l) 2,6-di-tert-butyl-4-methoxyphenol (2,6-DTBO).

Webster et al. reported the electrochemically controlled reversible transformation of α-TOH into its phenoxonium cation [3,6,8–10]. In their pioneering work, a combination of electrochemical and *in situ* spectroscopy experiments demonstrated that all redox states of α-TOH—capable of donating two electrons and one proton—are accessible in acetonitrile through the addition of an organic soluble acid or a Brønsted base coupled with electrochemical generation. As they showed, the stability of the redox states for α-TOH is related to its characteristic structure, which enables a quinone–hydroquinone π-conjugated redox system, despite its single hydroxyl group. Considering the structure–activity correlation of vitamin E in ROS elimination, it is reasonable that the differences in the four structures, α-, β-, γ-, and δ-TOH, are derived from those in the bulky methyl groups at the 5, 7, and 8 (R_1, R_2, and R_3) positions (Figure 1). The R_1, R_2, and *para*-oxygen respectively, are mainly considered to be related to the cyclic voltammetry responses, with the substituents determining the electron-donating ability and stability of tocopheroxyl radical ($TO^{\bullet}$) [3]. The differences in the electrochemical behavior of α-, β-, γ-, and δ-TOH were investigated, all of which were found to be similar, and showed little difference in the formal redox potentials of direct two-electron oxidation or oxidation of tocopheroxyl anions (TO^-) upon the addition of a Brønsted base [6]. However, there was a significant difference in the chemical reversibility of the redox behavior, suggesting that the stabilities of the produced intermediates, such as $TO^{\bullet}$ and phenoxonium cations, were different. The physicochemical properties confirmed by these electrochemical behaviors are presumed to be associated with electron transfer (ET) and proton transfer (PT) in the ROS elimination mechanism, but are not dominant to decide the reaction parameter between each ROS and TOH, particularly regarding the thermodynamics, kinetics, and deeper insights concerning the proton-coupled electron transfer (PCET) pathway, i.e., sequential PCET, hydrogen atom transfer involving the concerted PCET [11–16], and sequential proton loss electron transfer [5,17].

Referring to these studies, we investigated the electrochemical mechanism of the scavenging reaction of electrogenerated superoxide radical anion ($O_2^{\bullet-}$) by α-TOH in *N*,*N*-

Preprints (www.preprints.org) | NOT PEER-REVIEWED | Posted: 3 December 2021 doi:10.20944/preprints202112.0058.v1

dimethylformamide (DMF) [18]. Furthermore, a detailed mechanism was analyzed using density functional theory (DFT) calculations, and we proposed that the mechanism is a PCET characterized by the quinone–hydroquinone system (Equation (1)). In this mechanism, two PTs and one ET are thermodynamically preferred; the first PT from the acidic α-TOH to the $O_2^{\bullet-}$ forms α-TO^- and hydroperoxyl radical ($HO_2^{\bullet}$), followed by ET coupled with the second PT from another α-TOH. In our previous studies, it has been reported that $O_2^{\bullet-}$ is eliminated by polyphenols [18], diphenols (hydroquinone [19] and catechol [20]), and mono-phenols [21], through PCET mechanism. In these studies, the PCET mechanism based on quinone–hydroquinone π-conjugation involves two PTs and one ET for a successful $O_2^{\bullet-}$ elimination. The reversible cyclic voltammograms (CVs) in an alkali solution shown by Webster et al. revealed that PT is closely related to ET, and that the thermodynamically preferred mechanism of $O_2^{\bullet-}$ elimination is enabled by ET–PT coupling. It is reasonable to assume a similar PCET mechanism for β-, γ-, and δ-TOH involving two PTs and one ET between $O_2^{\bullet-}$ and two molecules of TOH since two protons are required in the net reaction (Equation (1)). However, the mechanism and structure–activity relationship of each TOH characterized by the methyl groups have not been provided.

$$O_2^{\bullet-} + 2\alpha\text{-TOH} \rightarrow H_2O_2 + \alpha\text{-TO}^{\bullet} + \alpha\text{-TO}^- \qquad \text{two PTs + one ET} \qquad (1)$$

In this study, we analyzed the reaction between electrogenerated $O_2^{\bullet-}$ and TOH in DMF, focusing on the structure–activity relationship of TOH on the $O_2^{\bullet-}$ elimination in relation to the PCET by electrochemistry and DFT calculation. Accordingly, we here present valuable information regarding the deeper mechanistic insight of PCET for the $O_2^{\bullet-}$ elimination reaction by TOH.

2. Materials and Methods

2.1.Chemicals

We obtained (+)-α-TOH (98.0%), (+)-β-TOH (98.0%), (+)-γ-TOH (96.0%), and (+)-δ-TOH (90.0%), from Sigma-Aldrich Inc (Tokyo, Japan), 2,2,5,7,8-pentamethyl-6-chromanol (97.0%), homogentisic acid γ-lactone (98.0%), 2,3-dihydro-2,2-dimethyl-7-hydroxybenzofuran (98.0%), trans-*para*-coumaric acid (98.0%), and phenol (99.5%), from Tokyo Chemical Industry Co., Ltd. (Tokyo, Japan), at the best available grade, and were used as received. 2,6-DTBP (98.0%), 2,6-DTBM (99.0%), TTBP (98.0%), and 2,6-DTBO (98.0%), were purchased from Tokyo Chemical Industry Co., Ltd., and recrystallized from benzene, and dried sufficiently under reduced pressure before use.

The solvent for electrochemical and electron spin resonance (ESR) spectral-measurements was spectrograde purity DMF available from Nacalai Tesque Inc. (Kyoto, Japan) and used as received. Tetrapropylammonium perchlorate (TPAP) was prepared as described previously [22] and used as a supporting electrolyte for DMF. Ferrocene (Fc), used as a potential reference compound, was commercially available from Nacalai Tesque Inc. and purified by repeated sublimation under reduced pressure immediately before use.

2.2.Electrochemical and In situ Electrolytic ESR Spectrum Measurements

Cyclicvoltammetry was performed with a three-electrode system comprising a glassy carbon (GC) working electrode, a coiled platinum counter electrode, and an $Ag/AgNO_3$ reference electrode (containing acetonitrile solution of 0.1 mol dm^{-3} tetrabutylammonium perchlorate and 0.01 mol dm^{-3} $AgNO_3$; BAS RE-5) at 25°C using a BAS 100B electrochemical workstation, coupled to a BAS electrochemical software to record data. *In situ* electrolytic ESR spectra were measured using a JEOL JES-FA200 X-band spectrometer. The controlled-potential electrolysis was performed at room temperature in an electrochemical ESR cell using a 0.5-mm-diameter straight Pt wire sealed in a glass capillary as a working electrode (Supplementary, Figure S1).

Samples were prepared in a glove box completely filled with dinitrogen (N_2) gas to prevent contamination by moisture. The DMF solution containing 0.1 mol dm^{-3} TPAP as a supporting electrolyte was saturated with O_2 by air-bubbling the gas for ca. 2−3 min and the gas was passed over the solutions during the electrochemical and ESR measurements

Preprints (www.preprints.org) | NOT PEER-REVIEWED | Posted: 3 December 2021 doi:10.20944/preprints202112.0058.v1

to maintain the concentration of O_2 at a constant level. The equilibrium concentration of O_2 was calculated as 4.8×10^{-3} mol dm^{-3}.

2.3.Calculation

All solution phase calculations were performed at the DFT level with the Becke three-parameter Lee–Yang–Parr (B3LYP) hybrid functional as implemented in Gaussian 16 Program package [23]. The geometry optimization, subsequent vibrational frequency calculations, and population analysis of each compound were performed by employing the standard split-valence triple ζ basis sets augmented by the polarization d,p and diffusion orbitals 6-311+G(d,p). The solvent contribution of DMF to the standard Gibbs free energies was computed employing the polarized continuum model (PCM) method at the default settings of the Gaussian 16, which is widely employed in the description of the thermodynamic characteristics of solvation. The zero-point energies and thermal correction, together with entropy, were used to convert the internal energies to standard Gibbs energy at 298.15 K. The natural bond orbital (NBO) technique was used for electron and spin calculations in population analysis [24].

3. Results

3.1. Cyclic Voltammetry and ESR Analysis of $O_2/O_2^{\bullet-}$ in the presence of TOH

In Figure 2, CVs of saturated O_2 (4.8×10^{-3} mol dm^{-3}) in the presence of TOH and related compounds (Figure 1(a–h)) in DMF are demonstrated. The CVs in the presence of (a) α-TOH and (e) 2,2,5,7,8-pentamethyl-6-chromanol, were already reported in our previous paper, although, are shown for comparison [18]. In aprotic solvents such as DMF, O_2 shows quasi-reversible redox (Equation (2)) corresponding to generation of $O_2^{\bullet-}$ in the initial cathodic scan and reoxidation to the starting materials (O_2), in the returned anodic scan (1c/1a, solid lines in Figure 2). The reversible CVs investigated here were all modified to irreversible one by the presence of any compounds (a–c, e–h) except (d) δ-TOH with concentration dependency (0 to 5.0, 10.0×10^{-3} mol dm^{-3}), similar to general phenolic compounds [18–21,25–28], supporting that CVs of bubbled N_2 showed no peak over the potential range. Thus, the loss of reversibility in the CVs of $O_2/O_2^{\bullet-}$ is caused by acid–base reaction, the initial PT from the compounds to $O_2^{\bullet-}$ as a Brønsted base forming $HO_2^{\bullet}$ (Equation (3)).

With the generation of $HO_2^{\bullet}$, bielectronic CVs were observed derives from the reduction of $HO_2^{\bullet}$ (Equation (4)) as shown in Figure 2(f–h), cathodic current 2c. Conversely, in the presence of (a–c, e) TOH, the bielectronic CVs don't appear due to the elimination of $HO_2^{\bullet}$ by the subsequent ET (Equation (5)) from the TO^-. In our previous study, the ET involved in the PCET mechanism for successful $O_2^{\bullet-}$ elimination required two structural characteristics; 1) the quinone–hydroquinone π-conjugated structure characterized by *ortho*/*para*-diphenol or aminophenol, and 2) the hydroxyl and amino proton for the second PT [18–21,27]. Notably, α-, β-, and γ-TOH showed the CV for the successful $O_2^{\bullet-}/HO_2^{\bullet}$ elimination, although the two structural characteristics are not involved in their structures.

$$O_2 + e^- \leftrightarrow O_2^{\bullet-} \qquad E^\circ = -1.284 \text{ V vs } Fc^+/Fc \qquad (2)$$

$$O_2^{\bullet-} + TOH \rightarrow HO_2^{\bullet} + TO^- \qquad \text{the initial PT} \qquad (3)$$

$$HO_2^{\bullet} + e^- \rightarrow HO_2^- \qquad E^\circ = -0.4 \text{ to } -0.2 \text{ V vs } Fc^+/Fc \qquad (4)$$

$$HO_2^{\bullet} + TO^- \rightarrow HO_2^- + TO^{\bullet} \qquad \text{ET} \qquad (5)$$

$$HO_2^- + TOH \rightarrow H_2O_2 + TO^- \qquad \text{the second PT} \qquad (6)$$

Preprints (www.preprints.org) | NOT PEER-REVIEWED | Posted: 3 December 2021 doi:10.20944/preprints202112.0058.v1

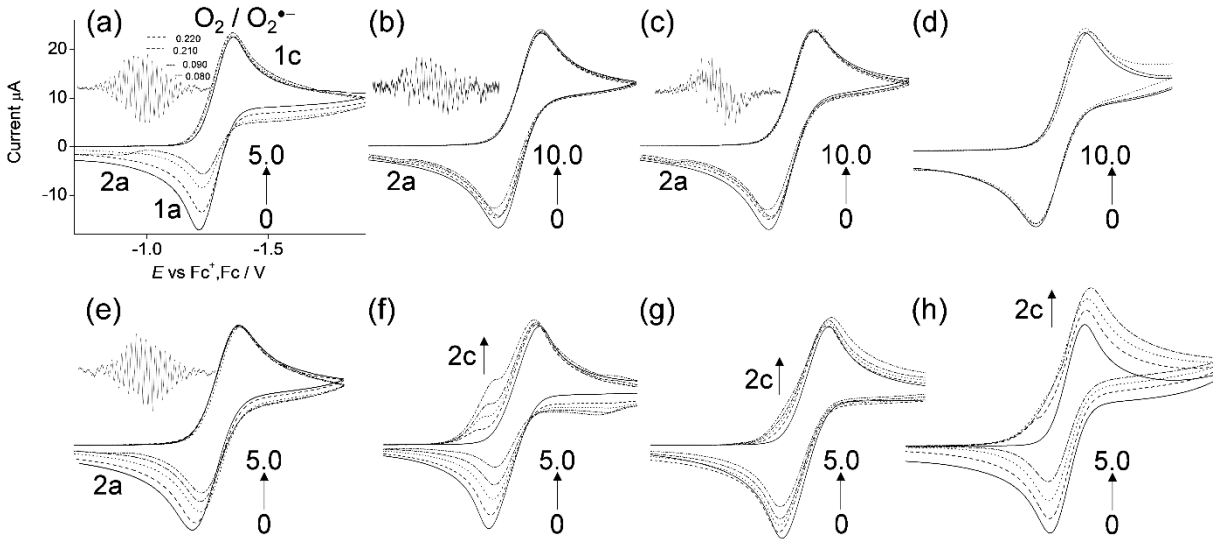

Figure 2. CVs of 4.8 × 10^{-3} mol dm^{-3} O_2 in the presence of (a–d) α-, β-, γ-, and δ-TOH, (e) 2,2,5,7,8-pentamethyl-6-chromanol, (f) homogentisic acid γ-lactone, (g) 2,3-dihydro-2,2-dimethyl-7-hydroxybenzofuran, and (h) trans-*para*-coumaric acid, in DMF containing 0.1 mol dm^{-3} TPAP recorded with a GC electrode at a scan rate of 0.1 V s^{-1}. Concentrations (× 10^{-3} mol dm^{-3}) are 0, 1.0, 2.0, 3.0, and 5.0 (a, e–h), and 0, 1.0, 2.0, 3.0, 5.0, and 10.0 (b–d) (the concentration changes are shown by arrows).

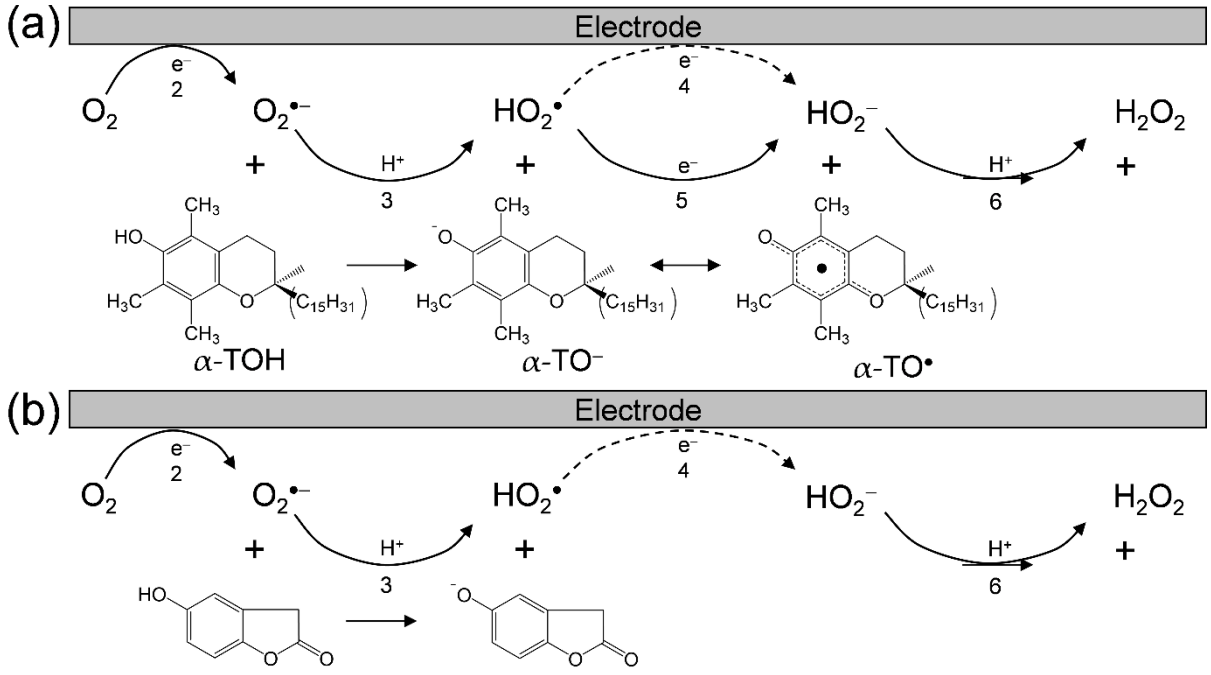

Figure 3. Plausible electrochemical mechanisms of $O_2/O_2^{\bullet-}$ in the presence of (a) α-TOH and (b) homogentisic acid γ-lactone in DMF. [1]The net PCET reaction between 2α-TOH and $O_2^{\bullet-}$ forming α-$TO^{\bullet}$, α-TO^-, and H_2O_2 involves two PTs and one ET, [2]one-electron reduction of $O_2/O_2^{\bullet-}$, [3]the initial PT from acidic substrate to $O_2^{\bullet-}$, [4]1-electron reduction of $HO_2^{\bullet}/HO_2^-$, [5]ET from substrate anion to $HO_2^{\bullet}$, [6]the second PT to HO_2^-.

Considering these results, we rationalized that $O_2^{\bullet-}$ formation after the primary electrode process associated with PT from the hydroxyl group leads to the irreversible overall reduction of O_2 to H_2O_2, which is driven by the exergonic reduction of the resulting $HO_2^{\bullet}/HO_2^-$. Therefore, the CV traces for $O_2/O_2^{\bullet-}$ in the presence of phenolic compounds are divided into two typical curves: type A, an irreversible two-electron process observed in electro–chemical–electro reactions (Equations (2)–(4)), and type B, an irreversible one-electron process (Equations (2), (3), (5), and (6)) leading to $O_2^{\bullet-}$ elimination. Figure 3 shows

Preprints (www.preprints.org) | NOT PEER-REVIEWED | Posted: 3 December 2021 doi:10.20944/preprints202112.0058.v1

the plausible electrochemical mechanism of $O_2/O_2^{\bullet-}$ in the presence of (a) α-TOH and in the presence of (b) homogentisic acid γ-lactone, summarizing Equations (2)–(6).

In this scenario, each CV result in the presence of α-, β-, γ-TOH, and 2,2,5,7,8-pentamethyl-6-chromanol, demonstrates type B (elimination of $O_2^{\bullet-}/HO_2^{\bullet}$). Conversely, the others demonstrate type A ($O_2^{\bullet-}$ is not eliminated) showing the appearance of a cathodic current ascribed to $HO_2^{\bullet}$. Then, the $O_2^{\bullet-}/HO_2^{\bullet}$ elimination by ET was confirmed via *in situ* electrolytic ESR measurements of the CV solutions at an applied potential of −1.3 V corresponding to the O_2 reduction (Equation (2)) with ESR scanning during 4 minutes. ESR spectra were obtained only for (Figure 2(a–c, e)) α-, β-, γ-TOH and 2,2,5,7,8-pentamethyl-6-chromanol (no ESR spectral for others). The two ESR spectra of (a) α-TOH and (e) 2,2,5,7,8-pentamethyl-6-chromanol with the simulated hyperfine coupling constants (hfcc) of hydrogen (a_H/mT, 0.220, 0.210, 0.090, and 0.080) [21], are identical, owing to the radical spin not being distributed on the 2-phytyl chain. For (b) β-TOH and (c) γ-TOH, a weak signal was observed, derived from their radicals [4,6,29,30]. With reference to (d) δ-TOH, ESR shows no signal and the CV shows minimal reactivity. The anodic peaks (2a) appearing in Figure 2(a–c, e) are inferred to be assigned to $TO^-/TO^{\bullet}$ oxidation, although the corresponding cathodic peak (reduction peak of $TO^{\bullet}$) is not observed. Based on the ESR results with the ratio of loss reversibility in CVs of $O_2/O_2^{\bullet-}$ (1a), the $O_2^{\bullet-}$ elimination ability can be estimated as the following order: (a) ~ (e) > (b) ~ (c). The CV and ESR results demonstrated that TOH (a–c, e) with their 6-chromanol ring and two or more methyl groups can eliminate $O_2^{\bullet-}/HO_2^{\bullet}$, whereas the other structural features contained in (f–h) and the phytyl chain in (a–d) are not effective. And, the number of the methyl group on the 6-chromanol ring is in good correlation with the $O_2^{\bullet-}$ elimination ability. These results imply that the reaction mechanisms of (b) β-TOH and (c) γ-TOH are the same as that of (a) α-TOH (Equation (1)); PCET involving two PTs and one ET, however their reactivities are different.

3.2. CV Analyses of the PCET Between $O_2^{\bullet-}$ and α-TOH Under Acid–base Interactions

To gain more insight into the mechanism, acid–base interactions of α-TOH in the CVs of $O_2/O_2^{\bullet-}$ were investigated. Figure 4a shows the CVs of 4.8 × 10^{-3} mol dm^{-3} O_2 in the presence of α-TOH at concentrations (×10^{-3} mol dm^{-3}) of 0, 1.0, 2.0, 3.0, and 5.0 (black line), and 7.0, 10.0, and 20.0 (red line). The bielectronic current (2c) on the peak of $O_2/O_2^{\bullet-}$ appears where the concentration is greater than 7.0. Then, a small anodic peak (2a) begins to become larger at concentrations greater than 7.0. These changes in the CV show that the electrochemical mechanism has changed at higher concentrations of α-TOH. Simultaneously, the reoxidation current of $O_2^{\bullet-}$ is not further decreased at concentrations over 7.0 ×10^{-3} mol dm^{-3}. Though the trigger of a series of reactions (type B) along with a generation of $TO^{\bullet}$ (Equation (5)) is the initial one-electron reduction of $O_2/O_2^{\bullet-}$ (Equation (2)), peak 2c (Figure 2a, red lines) will derive from the reduction of $TO^{\bullet}$, demonstrating that these peaks (2a/2c) can be attributed to $TO^{\bullet}/TO^-$.

In Figure 4b, CVs of α-TOH in the absence (black line) and the presence of 20.0 × 10^{-3} mol dm^{-3} sodium methoxide (red line) as a Brønsted base are shown. As reported by Wilson et al. [6], anodic oxidation of TO^- (3a) was observed to yield $TO^{\bullet}$ at a higher negative potential (E = −0.50 V vs Fc^+/Fc) than α-TOH (4a, E = 0.3 V vs Fc^+/Fc). Therefore, the resulting reversible peaks, 3a/3c, can be attributed to $TO^{\bullet}/TO^-$ redox couple. Similarly, α-TOH is deprotonated by $O_2^{\bullet-}$ forming TO^- (Equation (3)) in Figure 4a. However, the redox peaks of $TO^-/TO^{\bullet}$ are not observed at a lower concentration of α-TOH (black lines), owing to the following decomposition of $TO^{\bullet}$. Conversely, it is reasonable to assume that peak 2c/2a (redox of $TO^{\bullet}/TO^-$) is observable at higher concentration because TO^- is also produced via the second PT (Equation (6)) from another α-TOH molecule to HO_2^-.

Furthermore, in a faster scan rate at 1.0 V s^{-1} (Figure 4c), the reduction of $TO^{\bullet}/TO^-$ (peak 5c) was reversibly observable on the anodic and returned cathodic scans (second cycle), despite that $TO^{\bullet}$ is unstable. The redox potential of $TO^{\bullet}/TO^-$ is on the positive side of $O_2/O_2^{\bullet-}$, but a cathodic peak is not observed in the first cycle because that

Preprints (www.preprints.org) | NOT PEER-REVIEWED | Posted: 3 December 2021 doi:10.20944/preprints202112.0058.v1

α-TO$^{\bullet}$ is not generated at the potential before the reduction of $O_2/O_2^{\bullet-}$ (Equation (2)), which is the trigger of a series of reactions. Under those conditions; fast scan, a higher concentration of α-TOH for the second PT (Equation (6)), and in the second cycle, the reduction peak of α-TO$^{\bullet}$/α-TO^{-} is observable.

In aprotic solvents, the principal mode of α-TO$^{\bullet}$ decomposition occurs through a bimolecular self-reaction [8], where a hydrogen atom is transferred from the 5-methyl group of one α-TO$^{\bullet}$ to the phenoxyl oxygen atom of another α-TO$^{\bullet}$ (Equation (7)). The same mechanism (Equations (2, 3, and 5)) with the decomposition is expected for β-, γ-TOH, and 2,2,5,7,8-pentamethyl-6-chromanol, judging from both of the observed peak 2a in the CVs and the ESR spectra of TO$^{\bullet}$ (Figure 2(b–c, e)).

$$\alpha\text{-TO}^{\bullet} + \alpha\text{-TO}^{\bullet} \rightarrow \text{nonradical products} \quad (7)$$

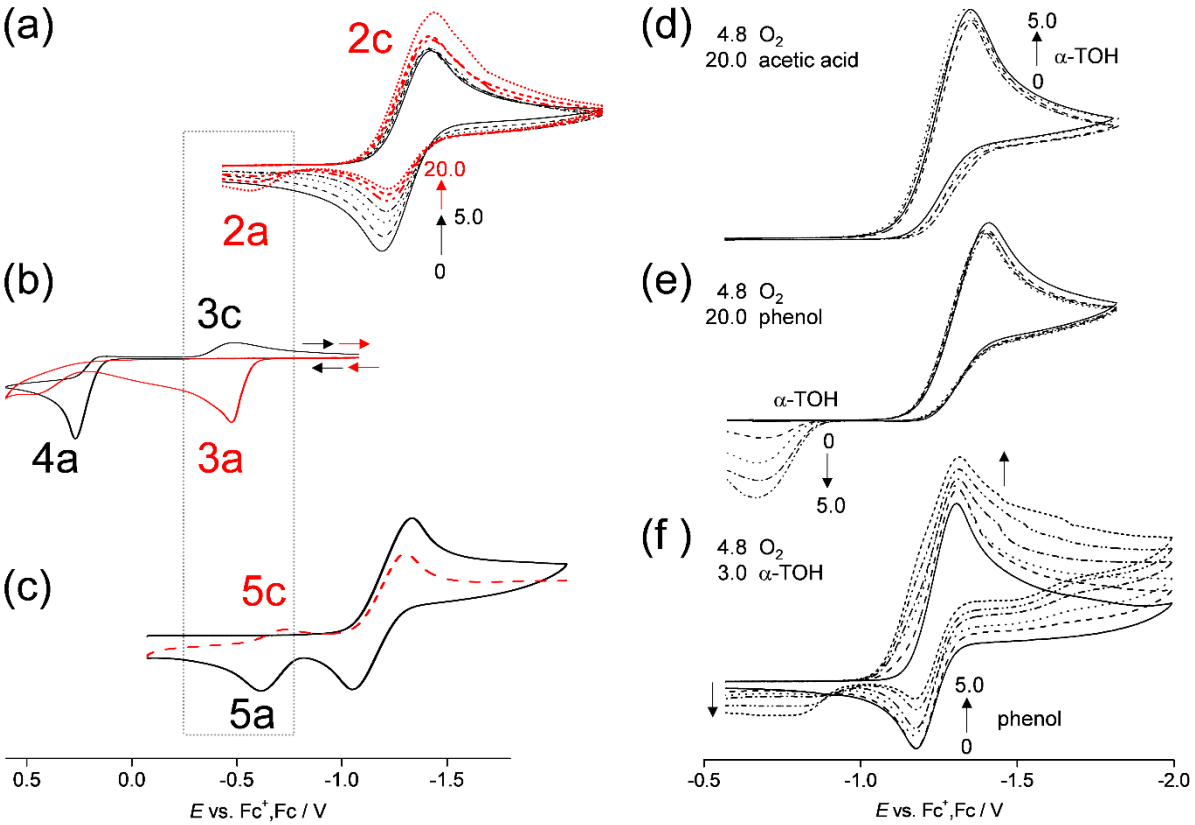

Figure 4. CVs of (a) O_2 in the presence of various concentrations (0, 1.0, 2.0, 3.0, 5.0, 10.0, and 20.0) of α-TOH, (b) α-TOH (5.0) in the absence (black line) and the presence of sodium methoxide (20.0, red line), (c) O_2 in the presence of α-TOH (7.0) for the first cycle (black line) and the second cathodic scan (red line), O_2 in the presence of both α-TOH (0, 1.0, 3.0, and 5.0) and (d) acetic acid (20.0), (e) phenol (20.0), and (f) O_2 in the presence of both α-TOH (3.0) and phenol (0, 1.0, 3.0, and 5.0), in DMF containing 0.1 mol dm^{-3} TPAP, recorded on a GC electrode (Φ = 1.0 mm) at scan rates of (a, b, d, e, and f) 0.1 and (c) 1.0 V s^{-1}. The concentration ($\times 10^{-3}$ mol dm^{-3}) changes are shown by the arrows.

Next, Figure 4(d–e) shows the CVs of saturated O_2 in the copresence of both 20.0 × 10^{-3} mol dm^{-3} proton donor ((d) acetic acid, (e) phenol) and 0–5.0 × 10^{-3} mol dm^{-3} α-TOH in a DMF solution. Irreversible bielectronic CVs of O_2 associated with PT are observed in the presence of a proton donor, respectively. The addition of α-TOH to the solution for (d) acetic acid shows minimal reactivity in the bielectronic CV, conversely, that for (e) phenol results in the appearance of a new anodic peak at approximately −0.55 V, with a good correlation of concentrations of α-TOH (0–3.0 × 10^{-3} mol dm^{-3}). Judging from the peak potential, the new peak is assigned to the oxidation of α-TO^{-}. In Figure 4f, the increasing concentration of phenol to the CV solution containing α-TOH (3.0 × 10^{-3} mol dm^{-3}) also resulted in the appearance of the anodic peak. Notably, the anodic peak only

Preprints (www.preprints.org) | NOT PEER-REVIEWED | Posted: 3 December 2021 doi:10.20944/preprints202112.0058.v1

appears in the copresence of all three chemical species ($O_2^{\bullet-}$, α-TOH, and phenol). Without phenol (Figure 4f, solid line), or without α-TOH (Figure 4e, solid line), no peak appeared around this potential range, as is the case without O_2. These results show that the π−planer ring of phenol supports the ET rather than proton donation in the intermolecular ET–PT: PCET. In the 1:2 mechanism shown in Equation (1), another molecule of α-TOH with its π−planer 6-chromanol ring will support the ET, as well as phenol.

3.3. Free Energy Calculations of PCET Between Electrogenerated $O_2^{\bullet-}$ and TOH

For a mechanistic analysis of the $O_2^{\bullet-}$ elimination by TOH in DMF, DFT calculations were performed at the (U)B3LYP/PCM/6-311+G(d,p) level. In Figure 5, the equilibrium scheme and standard Gibbs free energy changes ($\Delta G°$/kJ mol^{-1}, 298.15 K) of the six diabatic electronic states for the PCET involving two PTs and one ET between $O_2^{\bullet-}$ and two molecules of α-TOH (1:2) are shown. The important factors in determining the sequential processes shown in this scheme are the $\Delta G°$s for the acid–base interaction and the redox potentials of the components. ET1 ($\Delta G°$ = 325.9 kJ mol^{-1}) is strongly endergonic; thus, PT1 (70.3) forming α-TO^- to $HO_2^{\bullet}$ will primarily occur, as shown in the CV result. The $\Delta G°$s of the upper rectangle also show those of 1:1 reaction between $O_2^{\bullet-}$ and one molecule of α-TOH. Since the cathodic current of $HO_2^{\bullet}$ and the anodic current of α-TO^- was not observed in the CV (Figure 4a), where the concentration of α-TOH is less than 5.0, the 1:1 PCET reaction corresponding to the upper rectangle will be feasible, resulting formation of HO_2^- and α-$TO_2^{\bullet}$. On the other side, since the redox of α-TO^-/α-$TO^{\bullet}$ appeared in the CV at concentrations over 7.0 ×10^{-3} mol dm^{-3}, the 1:2 reaction; the initial PT (PT1) forming $HO_2^{\bullet}$ and following PCET corresponding to the lower rectangle, is feasible pathway. In the lower rectangle, PT3 (337.4) is strongly endergonic, thus, an exergonic ET2 (−50.3) followed by PT4 (−2.5) from another α-TOH is a thermodynamically feasible pathway.

For a comparative study, the $\Delta G°$ values of the PCET pathways for the other compounds were calculated (Table 1). From a thermodynamic viewpoint, the total values of $\Delta G°$ for the net PCET obtained from the sum of the values for the two PTs and one ET embody the energetic driving force of the net PCET. However, the total values cannot embody the energetic driving force because the $\Delta G°$ for the unfeasible single PT/ET has been summed in it. The important factor for the net PCET pathway comprised of PT1–ET2–PT4 to proceed as a sequential reaction is the $\Delta G°$ values of the individual reactions. In the pathway, the $\Delta G°$ of ET2 mainly constitutes an uphill energy barrier to the net PCET for homogentisic acid γ-lactone (20.7), 2,3-dihydro-2,2-dimethyl-7-hydroxybenzofuran (6.5), and trans-*para*-coumaric acid (155.8). Thus, these $\Delta G°$ values confirm that PCET is feasible for the 6-chromanol moiety in TOH but not for others, supporting the other experimental results. Furthermore, the $\Delta G°$s of ET2 for α-TOH (−50.3), β-TOH (−40.1), γ-TOH (−38.6), δ-TOH (−28.4), and 2,2,5,7,8-pentamethyl-6-chromanol (−49.1) are in good correlation with the ratio of loss reversibility in the CVs of $O_2/O_2^{\bullet-}$ in the presence of TOH (Figure 2(a–e)).

The $\Delta G°$s along the plausible pathway: PT1–ET2–PT4, indicate that the methyl groups on the 6-chromanol ring contribute to suppressing each of the PT (PT1, PT4) in the order of α- > β- > γ- > δ-TOH, and that in promoting ET2 in the same order. These results are thought to correspond to the increased electron density on the 6-chromanol ring with the electron-donating methyl group, thus suppressing PT and promoting ET. The increasing number of methyl group on the 6-chromanol ring promotes the total (net) PCET reaction, accelerating the CV modifications. These findings show that the key process in the net reaction pathway between $O_2^{\bullet-}$ and TOH is the ET2, which determines the structure–activity relationship of TOH on the $O_2^{\bullet-}$ elimination.

Preprints (www.preprints.org) | NOT PEER-REVIEWED | Posted: 3 December 2021 doi:10.20944/preprints202112.0058.v1

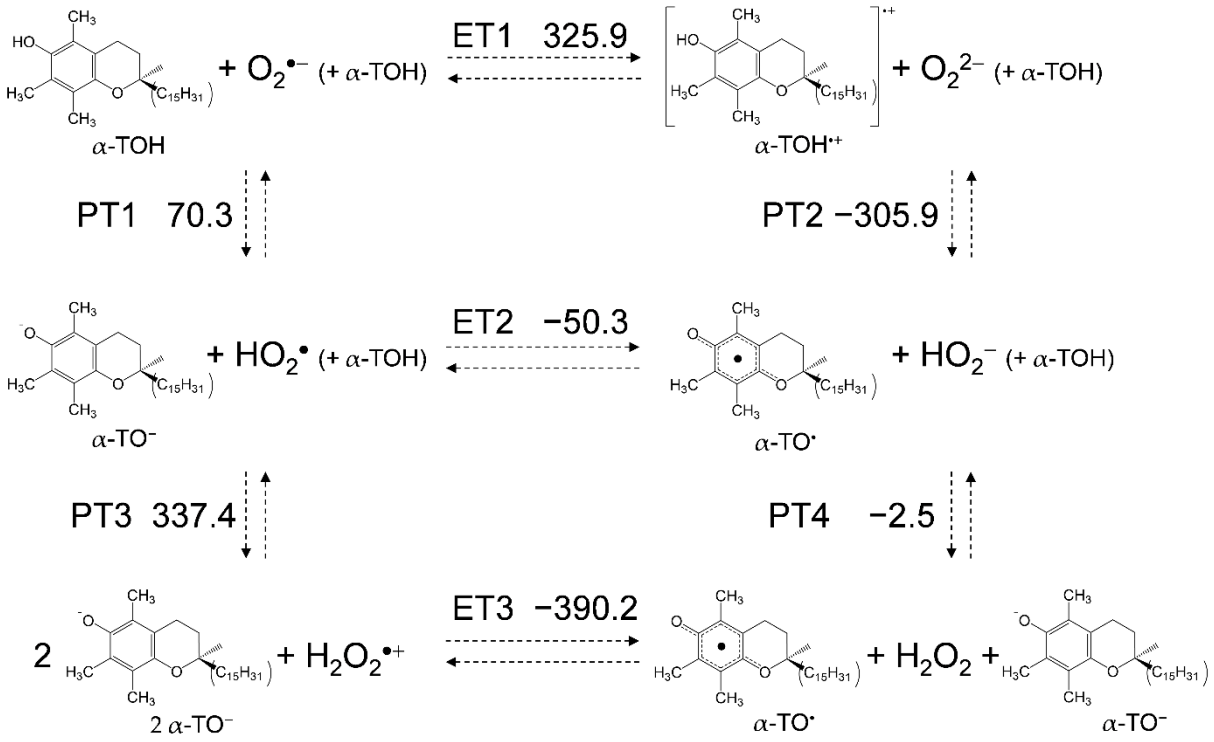

Figure 5. Six diabatic electronic states and the $\Delta G°$ values for PCET between α-TOH and $O_2^{\bullet-}$ involving two PTs and one ET in DMF. The $\Delta G°$ (kJ mol^{-1}, 298.15 K) for the (PT1-PT4) and ET (ET1-ET3) were calculated using DFT-(U)B3LYP/PCM/6-311+G(d,p) method.

Table 1. $\Delta G°$ values (kJ mol^{-1}, 298.15 K) for PCET between $O_2^{\bullet-}$ and TOH, and the related compounds in DMF, calculated using DFT at the (U)B3LYP/PCM/6-311+G(d,p) level.

Compounds	PT1	PT2	PT3	PT4	ET1	ET2	ET3	Total[1]
α-TOH	70.3	−305.9	337.4	−2.5	325.9	−50.3	−390.2	17.4
β-TOH	65.3	−303.4	332.4	−7.5	328.6	−40.1	−380.2	17.5
γ-TOH	62.9	−312.3	330.0	−9.9	336.6	−38.6	−378.5	14.4
δ-TOH	62.2	−308.6	329.2	−10.7	342.3	−28.4	−368.5	22.9
2,2,5,7,8-pentamethyl -6-chromanol	68.3	−306.3	335.4	−4.6	325.5	−49.1	−389.1	14.5
homogentisic acid γ-lactone	38.4	−349.4	305.5	−34.4	408.6	20.7	−319.2	24.8
2,3-dihydro-2,2-dimethyl -7-hydroxybenzofuran	48.3	−332.6	315.4	−37.6	387.4	6.5	−346.5	17.1
trans-*para*-coumaric acid	7.9	−249.6	275.0	−65.0	413.4	155.8	−184.1	98.7

[1] Total values involve the sum of $\Delta G°$s for two PTs and one ET.

After the initial PT along the plausible pathway (PT1–ET2–PT4) in Figure 5, α-TO$^-$, $HO_2^{\bullet}$, and α-TOH, are involved in the reaction system. Therefore, two reaction schemes for ET to $HO_2^{\bullet}$ and subsequent PT (PT4) is feasible, where electron donor is different; α-TOH or α-TO$^-$ as shown in Scheme 1. These two reaction schemes show that TOH, $HO_2^{\bullet}$ and TO$^-$, primarily form a HB complex centering an oxygen species (TO$^-$–$HO_2^{\bullet}$–TOH), and then transfer one proton and one electron. In the schemes, ET occurs between oxygen-π-orbitals orthogonal to the molecular framework, then, PT occurs between oxygen-σ-orbitals along the HBs. Besides a discussion on the concerted PCET or the sequential PCET, the two mechanisms (Scheme 1) are different in the direction of ET, (a) PCET; both ET and PT occur from the same molecule, and (b) intermolecular ET–PT (PCET in a broad sense); both ET and PT occur from different molecules. Calculated $\Delta G°$s suggest that the intermolecular ET–PT, ET (ET2) between α-TO$^-$ and $HO_2^{\bullet}$ (−50.3), is thermodynamically favorable rather than the PCET, ET between α-TOH and $HO_2^{\bullet}$ (100.7). Similar comparisons of

Preprints (www.preprints.org) | NOT PEER-REVIEWED | Posted: 3 December 2021 doi:10.20944/preprints202112.0058.v1

the ΔG°s for β-, γ-, and δ-TOH (Supplementary, Table S1) also showed thermodynamic superiority of (b) the intermolecular ET–PT, respectively.

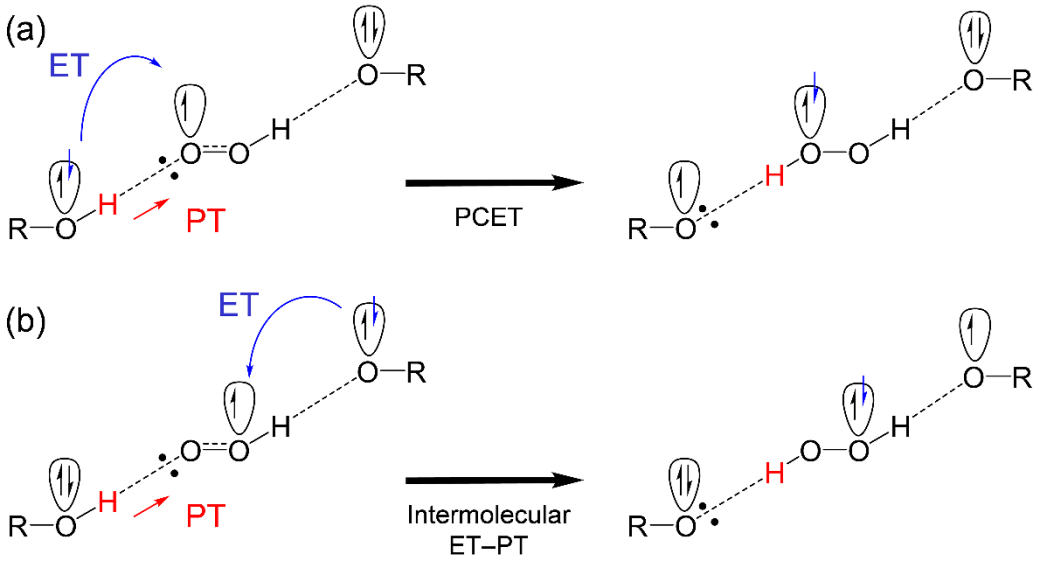

Scheme 1. Schemes of (a) PCET and (b) intermolecular ET–PT, between hydroxyl donor (ROH), corresponding anion (RO^-), and $HO_2^{\bullet-}$, formed after the initial PT.

3.4. Potential Energy Scanning for the Stable HB Complex Along the PCET

For gaining deeper insight into the structure–activity relationship on the PCET mechanism, potential energy surfaces were investigated with the frontier molecular orbital and NBO analyses at the (U)B3LYP/PCM/6-311+G(d,p) level of theory. It is assumed that the reaction involves three elementary steps: i) formation of the prereactive HB complex (PRC) from the free reactants, ii) reaction to the product complex (PC) via a transition state (TS), and iii) dissociation of the product complex yielding free products.

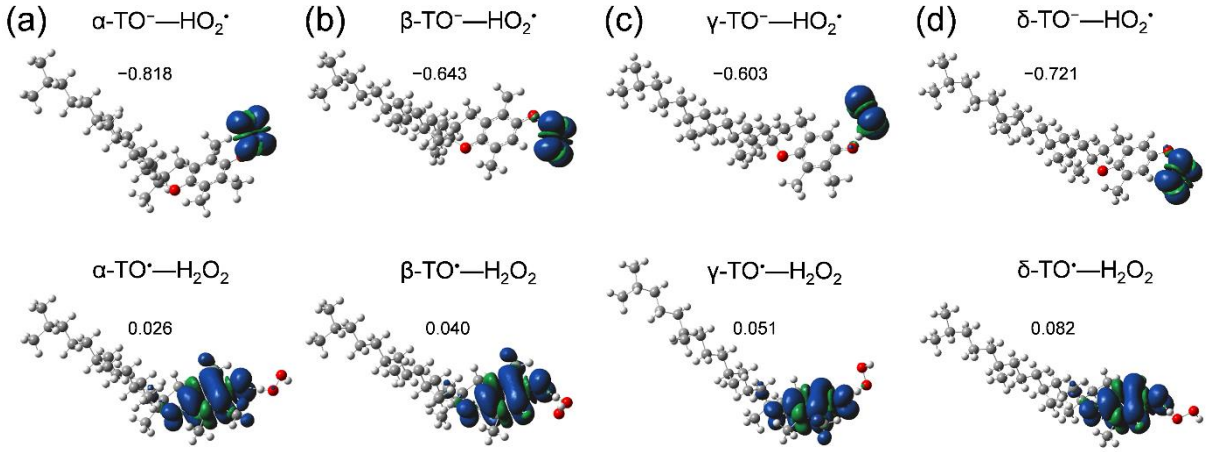

Figure 6. Optimized structure and spin distribution of HB complexes; TO^-—$HO_2^\bullet$ formed between TOH and $O_2^{\bullet-}$ (PRC), and $TO^\bullet$—H_2O_2 formed between TOH and $HO_2^\bullet$ in DMF, calculated using DFT-(U)B3LYP/PCM/6-311+G(d,p) method. Charges distributed on the TO^-/$TO^\bullet$ are denoted.

First, we start with an analysis of potential energy scanning for the stable HB complexes (PRC, intermediate HB complex, and PC) along the PCET reaction of α-, β-, γ-, and δ-TOH. Optimized structures of the 1:1 PRC (TOH–$O_2^{\bullet-}$) resulting TO^-–$HO_2^\bullet$ formed after the initial PT (in step, i)) were obtained (Figure 6, upper), but were not the PC ($TO^\bullet$–HO_2^-). Thus, potential energy surface along the following ET (step ii)) is not obtained, suggesting that 1:1 PCET reaction don't occur for all of α-, β-, γ-, and δ-TOH.

Preprints (www.preprints.org) | NOT PEER-REVIEWED | Posted: 3 December 2021 doi:10.20944/preprints202112.0058.v1

Similarly, optimization for both of the 1:2 PRC (TOH–$O_2^{\bullet-}$–TOH), the 1:2 PC (TO$^\bullet$–H_2O_2–TO^-), and the intermediate HB complex (TO^-–$HO_2^\bullet$–TOH) formed after the initial PT, centering an oxygen species bonded by a hydroxyl group of TOH were conducted. However, optimized stable structures of 1:2 HB complexes were not obtained, thus, their potential energy surfaces were not scanned. Since TOH have a long phytyl chain, it is difficult to form the 1:2 HB complexes. Conversely, the formation of HB complex between another molecule of TOH and $HO_2^\bullet$ formed after iii) dissociation of TO^-–$HO_2^\bullet$ complex can occur, resulting in formation of TO$^\bullet$–H_2O_2 (Figure 6, lower). Spins are distributed on the electron donor (TO$^\bullet$) side, demonstrating that ET coupled with the second PT (PCET) occurs. That is, the second PT from another molecule of β-, γ-TOH is necessary for the PCET, similar to α-TOH as reported in our previous study [18].

These results with the electrochemical results (Figures 2 and 3) reveal that β-, γ-TOH also bring about successful $O_2^{\bullet-}$ elimination through the 1:2 PCET involving two PTs and one ET. Although the potential energy surfaces of the 1:2 PCET (Scheme 1) were unclarified for both mechanisms; (a) PCET and (b) intermolecular ET–PT, the intermolecular ET–PT predominates in the $\Delta G°$ results. Alternatively, assuming that $HO_2^\bullet$ is released at a dissociation of the HB complex after the initial PT (TO^-–$HO_2^\bullet$), a 1:1 PCET between another TOH and $HO_2^\bullet$ can occur. The reaction coordinate along ET–PT via TS between TOH and $HO_2^\bullet$ can be found for α-, β-, γ-, and δ-TOH. However, the obtained activation energies (E_a, kJ mol^{-1}) of TS (Supplementary, Figure S3) are not in a good correlation with the ratio of loss reversibility in the CVs of $O_2/O_2^{\bullet-}$ (Figure 2). Considering these results, the 1:2 PCET mechanism for a successful $O_2^{\bullet-}$ elimination by β-TOH is shown in Figure 7; step i) formation of 1:2 PRC with the initial PT, followed by step ii) the intermolecular ET–PT, then step iii) dissociation of PC resulting formation of β-TO$^\bullet$, β-TO^-, and H_2O_2.

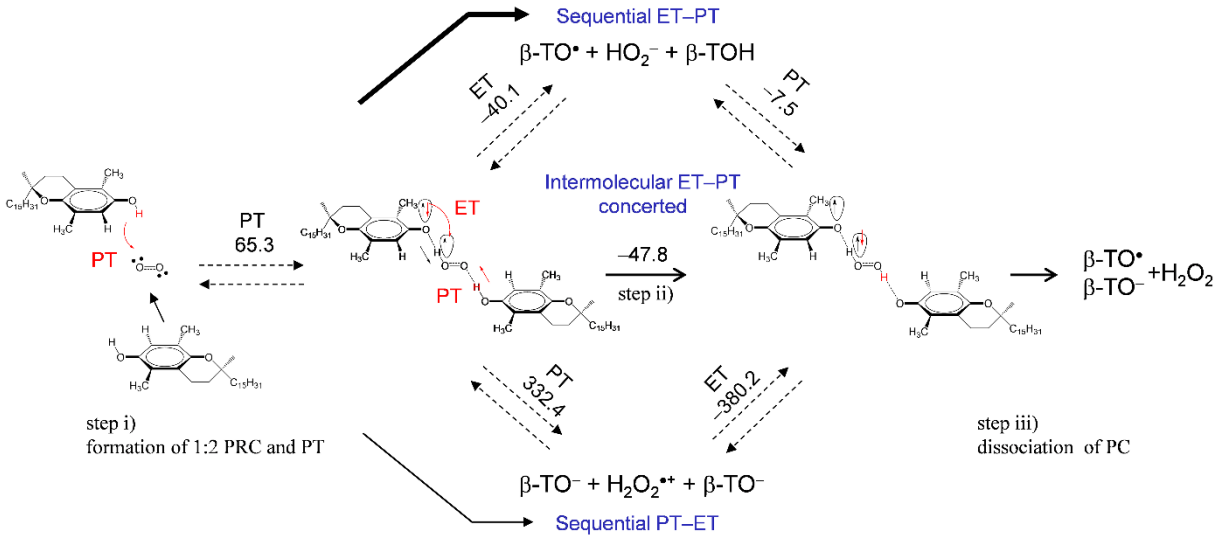

Figure 7. Plausible mechanism and the ΔG°s (kJ mol^{-1}, 298.15 K) for the PCET pathways between $O_2^{\bullet-}$ and β-TOH involving two PTs and one ET in DMF. The $\Delta G°$s were calculated using DFT-(U)B3LYP/PCM/6-311+G(d,p) method.

3.5. Effect of para-Oxygen in the 6-Chromanol Ring of TOH on the $O_2^{\bullet-}$ Elimination

To clarify the effect of the *para*-oxygen-atom in the 6-chromanol ring of TOH on the $O_2^{\bullet-}$ elimination, a comparative study using cyclicvoltammetry and *in situ* electrolytic ESR measurements of the O_2 in the presence of 2,6-DTBP, 2,6-DTBM, TTBP, and 2,6-DTBO was investigated. In Figure 8, the CVs of the $O_2/O_2^{\bullet-}$ are modified to irreversible two-electron CVs (type A) in the presence of the four phenolic compounds. Then, the ESR spectra were obtained in the presence of TTBP and 2,6-DTBO (Figure 8(c-d)). The observed spectra were assigned to their corresponding phenoxyl radicals (PhO$^\bullet$) [31,32]. The hfccs were simulated from the measured spectra, which confirm the generation of a PhO$^\bullet$ through the PCET involving one or two PT and one ET between the compounds and $O_2^{\bullet-}$. Conversely,

Preprints (www.preprints.org) | NOT PEER-REVIEWED | Posted: 3 December 2021 doi:10.20944/preprints202112.0058.v1

the CV and ESR results for (a) 2,6-DTBP and (b) 2,6-DTBM show that a PCET doesn't occur, although CV modifications caused by PT are observed. Another cathodic peak appears at (a) −0.5813, (b) −0.6577, (c) −0.6207, and (d) −0.8291 V, respectively, that is ascribed to the oxidation of the corresponding phenoxyl anion (PhO^-) to $PhO^\bullet$. In the CVs, the peak potentials of $PhO^\bullet/PhO^-$ are observed in the order; (a) 2,6-DTBP > (b) 2,6-DTBM, (c) 2,6-TTBP > (d) 2,6-DTBO (negative side). This order corresponds to the electron-donating ability of the *para*-substituted groups (-H > $-CH_3$, $-C(CH_3)_3$ > $-OCH_3$), known as the Hammett equation [33]. Furthermore, this order corresponds to the calculated standard redox potential ($E°$, V vs SHE) of $PhO^\bullet/PhO^-$ using eq. 8. In Table 2, from the potential difference vs $PhO^\bullet/PhO^-$ of 2,6-DTBP (ΔE, V vs E_{DTBP}), obtained from the $\Delta G°$ using DFT-(U)B3LYP/PCM/6-311+G(d,p) method.

$$\Delta G° = -zFE° \tag{8}$$

where z is the number of electrons (1), F is the Faraday constant (9.648533×10^4 C mol^{-1}).

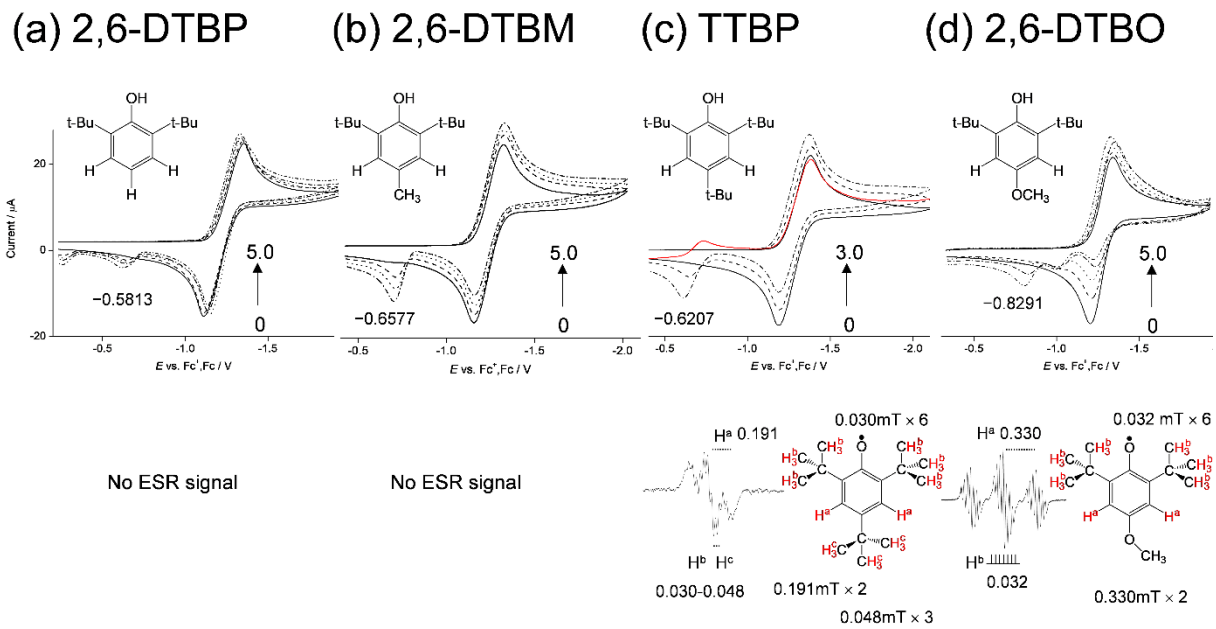

Figure 8. CVs of 4.8×10^{-3} mol dm^{-3} O_2 in the presence of (a) 2,6-DTBP, (b) 2,6-DTBM, (c) TTBP, and (d) 2,6-DTBO in DMF containing 0.1 mol dm^{-3} TPAP. The concentrations ($\times 10^{-3}$ mol dm^{-3}) are 0, 1.0, 3.0, and 5.0 (a, b, and d), and 0, 1.0, and 3.0 (c) (the concentration changes are shown by arrows). CVs were recorded with a GC electrode (Φ = 1.0 mm) at a scan rate of 0.1 V s^{-1}. ESR spectra of the CV solutions obtained by *in situ* electrolyzed system at an applied potential (−1.28 V vs Fc^+/Fc). The hfccs are obtained from a simulation of the experimental ESR spectra.

In the anodic scan for (d) 2,6-DTBO, two small peaks appeared on the positive side of the $O_2/O_2^{\bullet-}$ redox couple. It is unclear that which of the two peaks is assigned to $PhO^\bullet/PhO^-$. Notably, in the second cycle of the CV, the reduction peak of $PhO^\bullet$ is observable for (c) TTBP (red line) but not for (d) 2,6-DTBO, indicating that the $PhO^\bullet$ of TTBP is stable. Therefore, we infer that one of the anodic peaks for 2,6-DTBO arises from the decomposition of a radical. Moreover, an ESR spectrum is detectable for (c) TTBP but not for (b) 2,6-DTBM, although the potential of $PhO^\bullet/PhO^-$ for TTBP (−0.6207) is less negative than that for 2,6-DTBM (−0.6577) in both the experimental and calculated results. These results suggest that the thermodynamic properties of $PhO^\bullet$ (radical stability and redox potential) are not directly associated with the ET mechanism involved in the PCET, implying that the mechanism of the $O_2^{\bullet-}$ elimination involves a concerted ET–PT.

Furthermore, spins are distributed on the tertiary carbons of tertiary butyl (*t*-Bu) group but not on the combined carbons in the α-positions of 2 and 6 *t*-Bu groups of the

Preprints (www.preprints.org) | NOT PEER-REVIEWED | Posted: 3 December 2021 doi:10.20944/preprints202112.0058.v1

radicals (Figure 8(c-d)). For example, number of the line splitting observed in the ESR spectra for (d) 2,6-DTBO is 21 (3 · 7), the large 3 splitting is derived from two H^a, and the hyperfine 7 splitting corresponds to the number of combined six α-carbons (c). The largest coupling constants (0.191, 0.330 mT) are assigned to the two hydrogens at positions 3 and 5 in the phenolic ring of (c) TTBP and (d) 2,6-DTBO, respectively. Other hfccs are assigned to the *t*-Bu groups at positions 2, 4, and 6 in TTBP (0.048, 0.030 mT) and positions 2 and 6 in 2,6-DTBO (0.032 mT); however, the hydrogen atom (H^b) is not directly combined to tertiary carbons. The splitting corresponds to the number of combined α-carbons, suggesting that radical electrons are distributed only on tertiary carbons and the electronic spins resonate to the hydrogens (H^b) in the β-position. Thus, effect of *t*-Bu groups at positions 2 and 6 on the $O_2^{\bullet-}$ elimination is expected to be similar to that of the methyl group.

As a result of comparative analyses using the four 2,6-di-*t*-Bu-phenolic compounds, a higher electron-donating ability of the *para*-substituted group was required for the PCET, suggesting that the *para*-oxygen-atom in 6-chromanol ring of TOH is essential for successful $O_2^{\bullet-}$ elimination through the PCET.

Table 2. Standard redox potentials ($E°$, V vs SHE) of $PhO^{\bullet}/PhO^-$ of the compounds and ΔE (V vs E_{DTBP}) estimated from the calculated $\Delta\Delta G°$ (kJ mol^{-1}, 298.15 K) in DMF, calculated using DFT at the (U)B3LYP/PCM/6-311+G(d,p) level.

Compounds	[1] $\Delta\Delta G°$ (kJ mol^{-1})	[2] $E°$ (V vs SHE)	[3] ΔE (V vs E_{DTBP})
α-TOH	−349.3	3.620	−0.494
β-TOH	−359.5	3.726	−0.389
γ-TOH	−361.1	3.742	−0.373
δ-TOH	−371.2	3.847	−0.268
2,6-DTBP	−397.1	4.115	0
2,6-DTBM	−380.1	3.939	−0.176
TTBP	−381.6	3.955	−0.160
2,6-DTBO	−366.2	3.795	−0.319

[1] Difference between $\Delta G°$ of $PhO^{\bullet}$ and that of PhO^-. [2] The standard redox potentials of $PhO^{\bullet}/PhO^-$ vs standard hydrogen electrode (SHE) obtained from eq. 8. [3] $\Delta E°$ vs $PhO^{\bullet}/PhO^-$ of 2,6-DTBP.

4. Conclusions

In conclusion, we have shown the structure–activity relationship of α-, β-, γ-, and δ-TOH on the $O_2^{\bullet-}$ elimination through the PCET in DMF. As a result, we have clarified;

- β- and γ-TOH eliminates $O_2^{\bullet-}$ through the PCET involving two PTs and one ET, in a similar mechanism for α-TOH, conversely, δ-TOH does not
- the net PCET mechanism involves the initial PT with forming a 1:2 HB complex (TO^-–$HO_2^{\bullet}$–TOH) followed by intermolecular ET–PT as an intra-complex reaction
- the increasing number of methyl groups on a 6-chromanol ring promotes the PCET reaction, especially the latter ET–PT, increasing the electron-donating ability of the 6-chromanol ring
- the expansion of the π−conjugated plane via the 1:2 HB complex plays an important role in the PCET mechanism
- the electron-donating ability of the *para*-oxygen-atom in 6-chromanol ring of TOH is essential for successful $O_2^{\bullet-}$ elimination through the PCET

It was not clarified whether to proceed in a concerted PCET or a sequential PCET, however, the concerted pathway is reasonable for the findings that the net PCET involving the initial PT followed by intermolecular ET–PT occurs as an intra-complex reaction without dissociation of the HB complex.

Although the results presented in this manuscript are for a chemical reaction in aprotic DMF solvent rather than a biological system, the PCET theory is adaptable to biological processes involving both protic and aprotic conditions in such as a lipid bilayer. Therefore, we hope that the findings obtained in this study will provide evidence for the biological mechanistic actions of $O_2^{\bullet-}$ elimination by TOH.

Supplementary Materials: The following is available online at www.mdpi.com/xxx/s1, Figure S1: *in situ* electrolytic ESR system, Table S1: comparisons of $\Delta G°$s, Figure S2: change in the highest occupied molecular orbital-lowest unoccupied molecular orbital energies, Figure S3: energy profiles along ET–PT via TS between TOH and $HO_2^{\bullet}$, Figure S4: plausible PCET pathways between $O_2^{\bullet-}$ and α-TOH, Figure S5: plausible PCET pathways between $O_2^{\bullet-}$ and γ- TOH.

Author Contributions: Conceptualization, T.N.; data curation, R.H.; methodology, B.U.; resources, K.K.; supervision, S.U.; writing—original draft preparation, T.N.; writing—review and editing, B.U.; funding acquisition, T.N., R.H.

Funding: This research was funded by Grant-in-Aid for Scientific Research, grant number 19K16338 from Japan Society for the Promotion of Science (JSPS).

Conflicts of Interest: The authors declare no conflict of interest.

References

1. Sen, C.K.; Khanna, S.; Roy, S. Tocotrienols: Vitamin E beyond tocopherols. *Life Sci.* **2006**, *78*, 2088–2098, doi:10.1016/j.lfs.2005.12.001.
2. Sen, C.K.; Khanna, S.; Roy, S. Tocotrienols in health and disease: The other half of the natural vitamin E family. *Mol. Aspects Med.* **2007**, *28*, 692–728, doi:10.1016/j.mam.2007.03.001.
3. Lee, S.B.; Lin, C.Y.; Gill, P.M.W.; Webster, R.D. Transformation of α-tocopherol (vitamin E) and related chromanol model compounds into their phenoxonium ions by chemical oxidation with the nitrosonium cation. *J. Org. Chem.* **2005**, *70*, 10466–10473, doi:10.1021/jo0517951.
4. Lehtovuori, P.; Joela, H. Radical cations of vitamin E. *Phys. Chem. Chem. Phys.* **2002**, *4*, 1928–1933, doi:10.1039/b110970g.
5. Musialik, M.; Litwinienko, G. Scavenging of dpph• radicals by vitamin E is accelerated by its partial ionization: The role of sequential proton loss electron transfer. *Org. Lett.* **2005**, *7*, 4951–4954, doi:10.1021/ol051962j.
6. Wilson, G.J.; Lin, C.Y.; Webster, R.D. Significant differences in the electrochemical behavior of the α-, β-, γ-, and δ-tocopherols (vitamin E). *J. Phys. Chem. B* **2006**, *110*, 11540–11548, doi:10.1021/jp0604802.
7. Malyszko, J.; Karbarz, M. Electrochemical oxidation of trolox and α-tocopherol in acetic acid: A comparative study. *J. Electroanal. Chem.* **2006**, *595*, 136–144, doi:10.1016/j.jelechem.2006.07.018.
8. Williams, L.L.; Webster, R.D. Electrochemically controlled chemically reversible transformation of α-tocopherol (vitamin E) into its phenoxonium cation. *J. Am. Chem. Soc.* **2004**, *126*, 12441–12450, doi:10.1021/ja046648j.
9. Yao, W.W.; Peng, H.M.; Webster, R.D. Electrochemistry of α-tocopherol (Vitamin E) and α-tocopherol quinone films deposited on electrode surfaces in the presence and absence of lipid multilayers. *J. Phys. Chem. C* **2009**, *113*, 21805–21814, doi:10.1021/jp9079124.
10. Hong, M.P.; Webster, R.D. Investigation into phenoxonium cations produced during the electrochemical oxidation of chroman-6-ol and dihydrobenzofuran-5-ol substituted compounds. *J. Org. Chem.* **2008**, *73*, 2169–2175, doi:10.1021/jo702415q.
11. Wenger, O.S. Proton-coupled electron transfer with photoexcited metal complexes. *Acc. Chem. Res.* **2013**, *46*, 1517–1526, doi:10.1021/ar300289x.
12. Costentin, C.; Robert, M.; Savéant, J.M. Electrochemical and homogeneous proton-coupled electron transfers: Concerted pathways in the one-electron oxidation of a phenol coupled with an intramolecular amine-driven proton transfer. *J. Am. Chem. Soc.* **2006**, *128*, 552–4553, doi:10.1021/ja060527x.
13. Koper, M.T.M. Theory of the transition from sequential to concerted electrochemical proton-electron transfer. *Phys. Chem. Chem. Phys.* **2013**, *15*, 1399–1407, doi:10.1039/c2cp42369c.
14. Costentin, C.; Robert, M.; Savéant, J.M. Concerted proton-electron transfers: Electrochemical and related approaches. *Acc. Chem. Res.* **2010**, *43*, 1019–1029, doi:10.1021/ar9002812.

15. Hammes-Schiffer, S. Theory of proton-coupled electron transfer in energy conversion processes. *Acc. Chem. Res.* **2009**, *42*, 1881–1889, doi:10.1021/ar9001284.
16. Nakayama, T.; Okumura, N.; Uno, B. Complementary effect of intra- and intermolecular hydrogen bonds on electron transfer in β–hydroxy-anthraquinone derivatives. *J. Phys. Chem. B* **2020**, *124*, 848–860, doi:10.1021/acs.jpcb.9b10733.
17. Litwinienko, G.; Ingold, K.U. Solvent effects on the rates and mechanisms of reaction of phenols with free radicals. *Acc. Chem. Res.* **2007**, *40*, 222–230, doi:10.1021/ar0682029.
18. Nakayama, T.; Uno, B. Importance of proton-coupled electron transfer from natural phenolic compounds in superoxide scavenging. *Chem. Pharm. Bull. (Tokyo).* **2015**, *63*, 967–973, doi:10.1248/cpb.c15-00447.
19. Nakayama, T.; Uno, B. Quinone-hydroquinone π-conjugated redox reaction involving proton-coupled electron transfer plays an important role in scavenging superoxide by polyphenolic antioxidants. *Chem. Lett.* **2010**, *39*, 162–164, doi:10.1246/cl.2010.162.
20. Nakayama, T.; Uno, B. Concerted two-proton-coupled electron transfer from catechols to superoxide via hydrogen bonds. *Electrochim. Acta* **2016**, *208*, 304–309, doi:10.1016/j.electacta.2016.05.034.
21. Nakayama, T.; Uno, B. Structural properties of 4-substituted phenols capable of proton-coupled electron transfer to superoxide. *Int. J. Adv. Res. Chem. Sci.* **2016**, *3*, 11–19, doi:10.20431/2349-0403.0301002.
22. Okumura, N.; Uno, B. Electronic spectra of the electrogenerated 1,4-benzoquinone π-dianion and the strongly hydrogen-bonded charge-transfer complex with methanol. *Bull. Chem. Soc. Jpn.* **1999**, *72*, 1213–1217, doi:10.1246/bcsj.72.1213.
23. Frisch G. W.; Schlegel, H. B.; Scuseria, G. E.; Robb, M. A.; Cheeseman, J. R.; Scalmani, G.; Barone, V.; Petersson, G. A.; Nakatsuji, H.; Li, X.; Caricato, M.; Marenich, A. V.; Bloino, J.; Janesko, B. G.; Gomperts, R.; Mennucci, B.; Hratch, D. J., M.J.. T. *Gaussian 16, Rev. B.01*; 2016; ISBN 9781935522027.
24. Reed, A.E.; Weinstock, R.B.; Weinhold, F. Natural population analysis. *J. Chem. Phys.* **1985**, *83*, 735–746, doi:10.1063/1.449486.
25. Song, C.; Zhang, J. Electrocatalytic oxygen reduction reaction. In *PEM Fuel Cell Electrocatalysts and Catalyst Layers: Fundamentals and Applications*; 2008; pp. 89–134 ISBN 9781848009356.
26. Singh, P.S.; Evans, D.H. Study of the electrochemical reduction of dioxygen in acetonitrile in the presence of weak acids. *J. Phys. Chem. B* **2006**, *110*, 637–644, doi:10.1021/jp055296f.
27. Nakayama, T.; Honda, R. Electrochemical and mechanistic study of superoxide elimination by mesalazine through proton-coupled electron transfer. *Pharmaceuticals* **2021**, *14*, doi:10.3390/ph14020120.
28. Nakayama, T.; Honda, R. Electrochemical and Mechanistic Study of Oxidative Degradation of Favipiravir by Electrogenerated Superoxide through Proton-Coupled Electron Transfer. *ACS Omega* **2021**, *6*, 21730–21740, doi:10.1021/acsomega.1c03230.
29. Mukai, K.; Tsuzuki, N.; Ishizu, K.; Ouchi, S.; Fukuzawa, K. Electron spin resonance and electron nuclear double resonance studies of cation radicals derived from tocopherol model compounds. *Chem. Phys. Lipids* **1984**, *35*, 199–208, doi:10.1016/0009-3084(84)90046-X.
30. Matsuo, M.; Matsumoto, S. Electron spin resonance spectra of the chromanoxyl radicals derived from tocopherols (vitamin E) and their related compounds. *Lipids* **1983**, *18*, 81–86, doi:10.1007/BF02534695.
31. Valoti, M.; Sipe, H.J.; Sgaragli, G.; Mason, R.P. Free radical intermediates during peroxidase oxidation of 2-t-butyl-4-methoxyphenol, 2,6-di-t-butyl-4-methylphenol, and related phenol compounds. *Arch. Biochem. Biophys.* **1989**, *269*, 423–432, doi:10.1016/0003-9861(89)90126-4.
32. Mukai, K.; Nishiguchi, H.; Ishizu, K.; Deguchi, Y.; Takaki, H. Solvent Effects in the Electron Spin Resonance Spectra of Some Phenoxyl, Nitroxide, and Anilino Radicals. *Bull. Chem. Soc. Jpn.* **1967**, *40*, 2731–2739, doi:10.1246/bcsj.40.2731.
33. Hammett, L.P. The Effect of Structure upon the Reactions of Organic Compounds. Benzene Derivatives. *J. Am. Chem. Soc.* **1937**, *59*, 96–103, doi:10.1021/ja01280a022.